Energy and Exergy Evaluation of High-Temperature Vapor-Injection Heat Pumps Applied to a Reboiler of a Carbon Capture Pilot Plant

Joy Surjy Deb[a,b], Brieuc Beguin[a], Ward de Paepe[c], Vincent Lemort[b] and Grégoire Léonard[a]

[a] *Chemical Engineering, Université de Liège, Liège, Belgium, JS.Deb@uliege.be, CA*
[b] *Thermodynamics Laboratory, Aerospace and Mechanical Engineering, Université de Liège, Liège, Belgium,*
[c] *Thermal Engineering & Combustion Unit, Université de Mons, Mons, Belgium.*

Abstract:

In amine-based CO_2 capture systems, the reboiler represents the main thermal demand for solvent regeneration and is conventionally supplied by steam or, sometimes by electrical resistance, leading to high electricity consumption and exergy losses. High-temperature heat pumps offer an alternative by upgrading low-grade waste heat to the required temperature level. However, limited work addresses the integration of vapor-injection high-temperature heat pumps in amine-based CO_2 capture pilot plants under realistic waste-heat constraints and combined energy and exergy assessment. The district heating network at the Sart-Tilman campus and the University of Liège Hospital is supplied by a centralized biomass-fired combined heat and power plant (CHP). An amine-based CO_2 capture mobile pilot plant with electric reboiler is being developed at the site as a demonstration platform, with the CHP plant as its first industrial host unit. In this context, a high-temperature vapor-injection heat pump is investigated for integration into the pilot plant to replace the electric reboiler by recovering and upgrading internally available low-grade waste heat to about 120°C. The analysis is based on steady-state simulations combining process modeling in Aspen Plus and heat pump modeling in Python. Internal hot process streams provide recoverable waste heat between 40°C and 105°C approximately. The associated cooling water streams, after mixing, are available at around 40°C and serve as the heat source for the heat pump. Two vapor-injection heat pump architectures using R-1233zd(E) are compared: a flash-tank-based configuration and a configuration with an intermediate evaporator. The condensing temperature is fixed at 130°C, while a parametric study identifies an optimal evaporating temperature of around 29–30°C. Results demonstrate that the flash-tank configuration provides superior performance, with COP values of 1.82–2.24 compared to 1.8–2.14 for the two-evaporators configuration, along with lower exergy losses across operating points. Overall, this study confirms feasibility and analyzes performance dependence on operating conditions and architecture.

Keywords:

CO_2 Capture; Exergy Analysis; High-Temperature Heat Pump; Process Heat Integration; Vapor-Injection Heat Pump.

1. Introduction

One of the most pressing global problems is climate change, which occurs due to higher greenhouse gas emissions. The Paris Climate Agreement aims at limiting global warming to 1.5°C, while keeping it well below 2°C [1]; therefore, there should be a considerable reduction in CO_2 emissions. In this case, the European Union has pledged to reach net-zero emissions and a carbon-neutral economy by 2050 [2]. While many low- and zero-carbon technologies are available, their implementation is often limited by high costs and system complexity [3]. Among the existing technologies, Carbon Capture, Utilization and Storage (CCUS) can be considered a technology to decrease CO_2 emissions from industrial enterprises. It will be challenging to meet climate goals without CCUS [4-5], which can be applied particularly in the cement, steel, petrochemicals, and pulp and paper industries.

Among numerous CO_2 capture technologies, absorption-regeneration loop with liquid solvents appears as the most mature one, especially with amine-based solvents. In such systems, the stripper column is the most energy-intensive unit, as it requires significant thermal energy to desorb CO_2 from the solvent. Conventionally, this heat is supplied by steam through a reboiler, which involves multiple energy conversion stages and associated efficiency losses. Electric heating may also be considered; however, it leads to substantial exergy destruction and high electrical consumption due to the direct conversion of high-grade energy into low-temperature heat. Previous studies [6–8] have shown that heat pump-based configurations can outperform conventional heat supply options such as natural gas-fired systems (e.g., combined cycle plants), boilers, and biomass-based systems. In addition, the CO_2 capture process inherently rejects low-grade heat through

several cooling units, which can be recovered and upgraded using a high-temperature heat pump to supply the reboiler.

The definition of a high-temperature heat pump varies in the literature; however, systems delivering heat above 100°C are generally classified as such [9]. Several studies [10–12] have investigated different heat pump configurations and refrigerants to improve performance under high-temperature conditions. For instance, Arpagaus et al. [11] analyzed multiple configurations, including internal heat exchangers, economizers, flash tanks, and cascade systems, while another study [12] compared vapor-injection and multi-stage compression systems under high pressure ratios. Despite these advances, the selection of the most suitable heat pump architecture remains highly dependent on process-specific temperature levels and heat availability, making it a case-dependent problem. However, limited work has addressed the process-specific integration of vapor-injection high-temperature heat pumps in amine-based CO_2 capture pilot plants, particularly under realistic waste-heat temperature constraints and with a combined energy and exergy assessment.

In this context, high-temperature vapor-injection heat pumps are investigated as an alternative to electric resistive heating for supplying the reboiler duty of an amine-based CO_2 capture pilot plant. The system is designed to deliver approximately 47.7 kW at a temperature level around 120°C by recovering and upgrading internally available low-grade waste heat. The objective of this work is to evaluate the feasibility of replacing the electric reboiler with such a system and to identify the most suitable heat pump configuration based on energy and exergy performance. The main contributions of this work can be summarized as follows:

- Integration of internally available process waste-heat into a high-temperature vapor-injection heat pump for reboiler heat supply.
- Comparative evaluation of two vapor-injection heat pump architectures under process-specific operating conditions and varying intermediate pressure of the heat pump.
- Combined energy and exergy analysis of the proposed architectures.

2. Methodology and System Modeling

This section describes the integrated modeling framework developed in this study. In this study the analysis is based on steady-state simulations combining process modeling in Aspen Plus and thermodynamic heat pump modeling in Python. The CO_2 capture process is modelled in Aspen Plus to define temperature levels and waste heat availability, which are subsequently used to constrain and evaluate the heat pump configurations.

2.1 CO_2 Capture Pilot Plant

The Sart Tilman campus and the University of Liège hospital are supplied by a district heating network whose base load is covered by a biomass-fired combined heat and power (CHP) plant. This facility, in operation since 2012, provides both heat and electricity to the site, meeting around 60 % of the total heat demand [13]. An amine-based mobile pilot plant is under construction, and the CHP facility is the first industrial site where it will be tested. In the mobile pilot plant, the reboiler duty is initially supplied by electric resistance heaters to enable plug-and-play operation.

2.2 Aspen Plus Modeling of the Capture Process

The pilot plant has been modelled by Aspen Plus. The process-side results are obtained from an Aspen Plus model developed in-house within the framework of the CO_2 capture pilot plant by project collaborators. The Aspen Plus model has been developed and validated independently [14] within the project, ensuring realistic process-side boundary conditions for the heat pump integration. This model provides the reboiler duty, as well as the heat duties and temperature levels of the available hot and cold process streams, which are used as boundary conditions for the present study. The pilot project will capture approximately one ton of CO_2 daily, with a maximum flue gas flow rate of approximately 360 kg/h. However, the reboiler heat duty and operating temperature of the stripper vary based on the operating pressure [15]. Therefore, among operating parameters, stripper pressure is set to 2 bar as a trade-off between decreased reboiler heat duty and increased thermal degradation at higher pressures. Under this condition, corresponding to a capture rate of 90%, the required reboiler heat duty of the stripper is approximately 47.7 kW at around 120 °C, as obtained from the Aspen Plus simulation, and must be supplied by the heat pump condenser.

2.3 Waste Heat Availability and Heat Source Characterization

According to the Aspen Plus model, four main internal process units as illustrated in Fig.1 need to be cooled till certain temperature and thus generate significant recoverable waste heat at temperature levels ranging approximately from 40°C to 105°C, corresponding to a total thermal potential of about 68 kW before losses. Though in the real pilot plant the heat exchangers will be well insulated, to account for unavoidable heat losses during heat recovery and transfer, a conservative loss factor of 10% is applied for each process streams, reducing the recoverable waste heat to approximately 61.5 kW available for the heat pump.

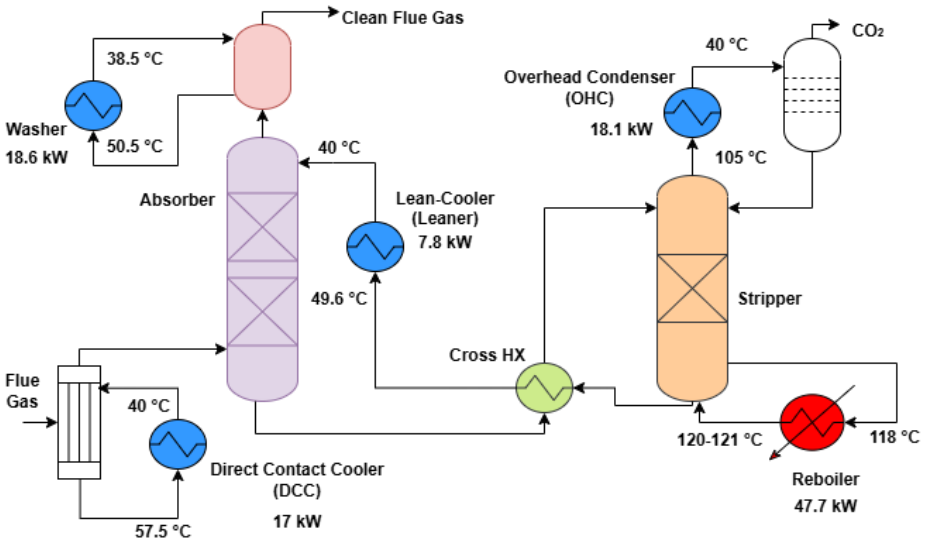

Figure 1. Plant's Heat Duties with Available Hot Streams and Reboiler

Without heat pump integration, all streams are cooled by a common cooling-water loop that splits into four branches, each removing heat from a process stream, in total 61.5 kW after considering losses. The cooling water streams then recombine, and the resulting mixture typically reaches 40°C and subsequently rejects all the heat in an air cooler before returning to the system at around 30°C. The cooling water circuit acts as a stable low-temperature heat source for the heat pump evaporator. After the heat extraction process, the water is cooled in the air cooler before being reused. As expected, extracting heat from the cooling circuit reduces the cooling load of the air cooler, thereby lowering its power consumption. Based on these operating conditions and available heat sources, a high-temperature heat pump system is designed and analyzed.

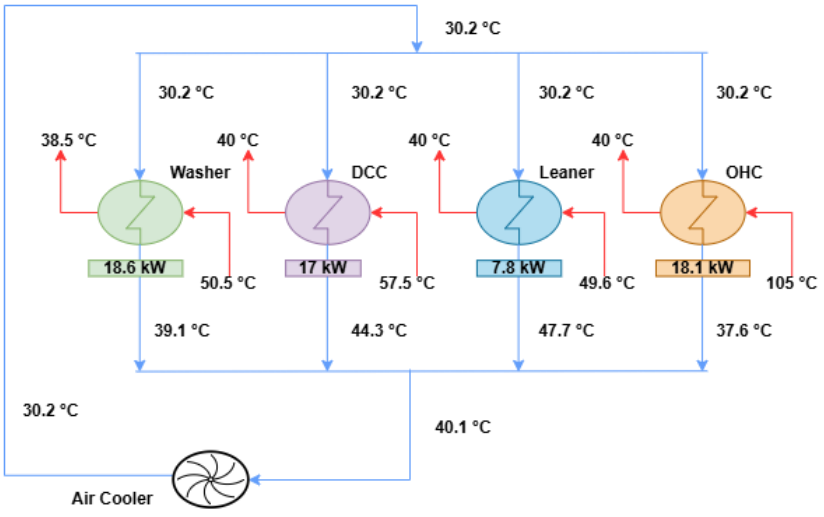

Figure 2. Plant's Cooling Water Network

2.4 Heat Pump

In this section the heat pump modeling, plant's heat integration, different components of the heat pump and architecture are discussed.

2.4.1 Refrigerant

R-1233zd(E) is selected as a suitable working fluid due to its low Global Warming Potential (GWP) 1 and Ozone Depletion Potential (ODP) 0.00034, non-flammability (A1 classification), high critical temperature (166°C), and favourable thermodynamic properties for high-temperature applications [16 –17].

2.4.2 Compressor

Advanced heat pump configurations often include multiple stages, compressors, and components such as flash tanks and economizers. While these can improve performance, they are not always practical due to limited market availability, especially dual-stage compressors requiring very low displacement at high pressure. Considering technical feasibility, space constraints, and equipment availability, a single-compressor vapor-injection configuration is selected as a practical compromise between simplicity and performance. The chosen

scroll compressor, Copeland ZW650HUH, can operate up to 135°C and has a swept volume of ~440 $cm^3 \cdot rev^{-1}$. This is the only compressor that we could identify following a market study considering high discharge temperature and heating capacity. Though the swept volume is fixed, the compressor speed can be varied to adjust the suction mass flow rate. The available performance data is limited; therefore, few assumptions were made. One study [18] with the same compressor reported operation at 50–60°C source and ~120°C sink (60–70 K lift), with isentropic efficiency around 70–72% and total efficiency ~63%. Based on this, a conservative isentropic efficiency of 65% is used in the model, consistent with literature values for high-temperature applications [16,18] and volumetric efficiency is assumed to be 0.9. While full validation is not yet possible, the assumptions follow established trends. This work establishes the basis for the design and implementation of a high-temperature heat pump system, with future efforts focusing on experimental validation in the pilot plant.

2.4.3 Architecture

Two vapor-injection heat pump architectures are analyzed and compared, as illustrated in Fig. 3. In the first architecture (Fig. 3a), injection vapor is generated using a flash tank. In the second configuration (Fig. 3b), it is supplied by a second evaporator operating at an intermediate temperature level.

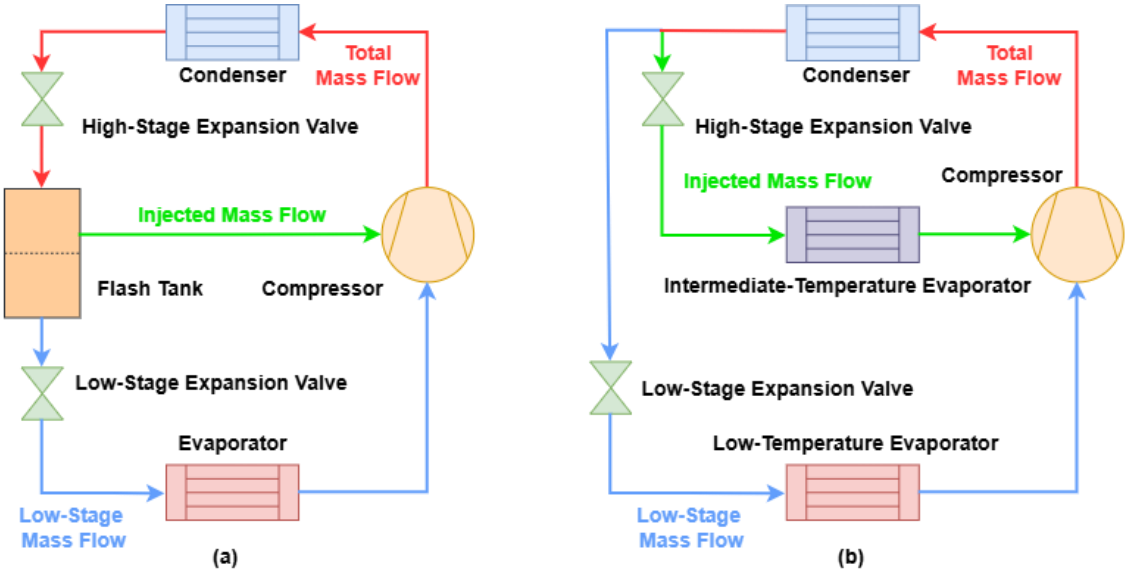

Figure 3. Heat Pump Architecture: (a) Flash-Tank Architecture; (b) Two-Evaporators Architecture

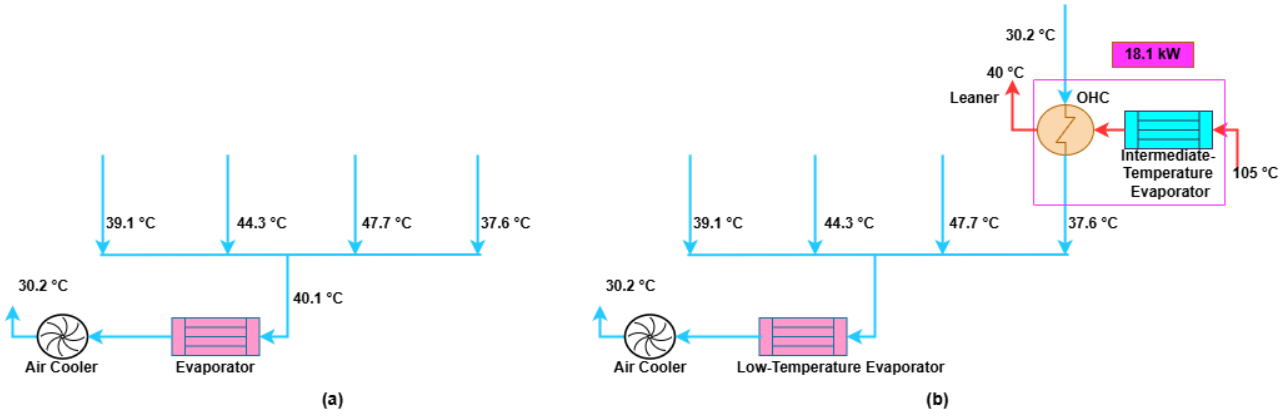

Figure 4. Evaporators Position: (a) Flash-Tank Architecture; (b) Two-Evaporators Architecture

In the flash-tank architecture, there is only one evaporator, and it is placed in the mixed cooling water stream, before the air cooler as illustrated in Fig. 4(a). Whereas, for the two-evaporators architecture in Fig. 4(b), the flash tank is replaced by an intermediate-temperature evaporator in order to utilize the available higher-temperature OHC heat source within the process as shown in Fig. 5. This modification allows part of the heat demand to be supplied at a higher temperature level, thereby lowering exergy destruction within the system. Among the hot streams illustrated in Fig. 1, the OHC hot stream is the most relevant. This is particularly important for the two-evaporators configuration due to its wide temperature range and non-linear T–Q profile, as illustrated in Fig. 5, resulting from its multicomponent nature (water–CO_2 mixture).

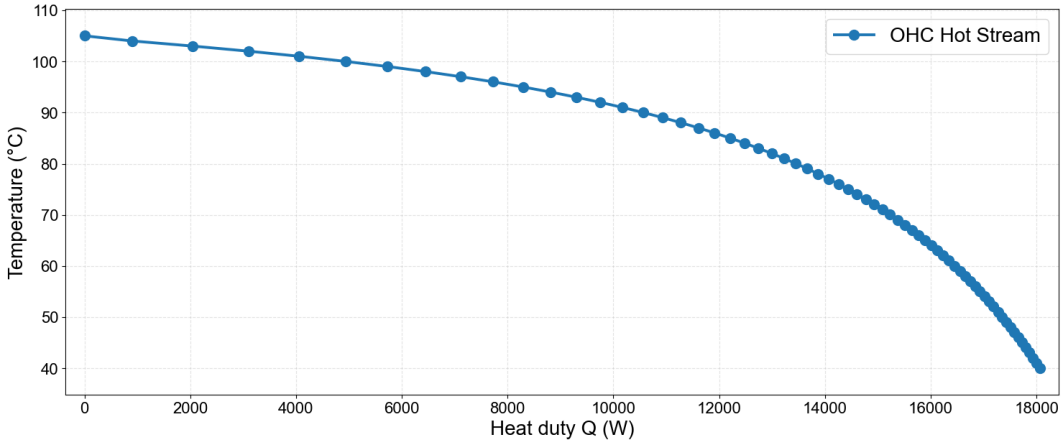

Figure 5. T–Q Curve of Overhead Condenser (OHC) Hot Stream

This stream provides significant heat over both high to low temperature levels, enabling its effective utilization in a two-stage evaporation process and allowing part of the heat demand to be supplied at a higher temperature level, thereby reducing exergy destruction. In this configuration, part of the OHC stream is utilized in the intermediate evaporator, while the remaining heat is transferred to the water loop. The recoverable heat from the OHC hot stream depends on its temperature–heat profile, i.e., the extent to which the stream is cooled as shown in Fig.5. The saturation pressure in the intermediate evaporator determines the refrigerant saturation temperature and, with a fixed pinch of 5 K, sets the minimum outlet temperature of the OHC hot stream. As the intermediate pressure increases, the allowable outlet temperature rises, reducing the cooling range and thus the heat recovered in the intermediate evaporator. Consequently, the remaining heat is redirected to the water loop, leading to slight variations in the mixing temperature, although this effect remains limited due to adjustment of the cooling water mass flow rate.

2.4.4 Assumptions, Methodology and Operating Conditions

The heat pump cycle is modeled in steady-state regime with Python, using thermophysical properties of R-1233zd(E) from CoolProp database. The system includes the compressor, condenser, evaporator, expansion devices, and either a flash tank or a second intermediate-temperature evaporator depending on the configuration. The expansion valves are modeled as isenthalpic processes, and vapor mixing in the compressor at the intermediate pressure level is assumed to be isobaric. A constant minimum temperature pinch of 5 K is maintained for all evaporators and condenser, and a superheat of 5 K is imposed for all evaporators across both architectures. All heat exchangers are considered counter flow.

The reboiler requires a temperature of about 120°C. With a 5 K pinch, the outlet of the refrigerant from condenser must be at least 125°C. In addition, with 5 K subcooling, the minimum condensing temperature is consequentially 130°C (~19 bar). As mentioned earlier, the maximum discharge temperature of the compressor is 135°C. Therefore, the condensing temperature is set to its minimum allowed limit of 130°C and thus outlet is fixed at 125°C. However, the discharge temperature varies based on each simulation. A combined heat loss of 10% is considered on the evaporator side to account for losses from the hot process streams to the cooling water and from the cooling water to the evaporator, and total available heat for heat pump's evaporator is 61.5 kW as described in Section 2.3.

The compressor's swept volume is fixed as of ~440 $cm^3 \cdot rev^{-1}$ but the frequency is varied and thus the suction mass flow rate is varied during each simulation. The vapor-injection compressor is modeled as two compression stages in series with intermediate injection and isobaric mixing, with a constant isentropic efficiency of 65% assumed for each stage, including an additional 5% heat loss in the discharge line. On the condenser side, a further 10% heat loss is included to represent losses between the condensing refrigerant and the stripper fluid in the reboiler. As a result, the effective condenser heating capacity is 53 kW, which is used for the calculation of the coefficient of performance (COP).

A parametric study is conducted to determine the optimal maximum saturation temperature of the single evaporator for flash-tank architecture or the low-temperature evaporator for the second architecture. Considering a superheat of 5 K and a minimum pinch of 5 K, the evaporating temperature is constrained by the available heat source. For each selected evaporating temperature, the cooling water outlet temperature is calculated to verify that the pinch condition is satisfied; otherwise, the operating point is rejected. A parametric study is then carried out to identify the optimal evaporating temperature based on the COP.

$$COP = \frac{53\ kW}{Total\ Electrical\ Power\ Input\ to\ the\ Compressor} \quad (1)$$

As shown in Fig. 6, the optimal evaporating temperature is approximately 29 °C for flash-tank architecture and 30 °C for the two-evaporators architecture. Above these values, the required heat duty cannot be achieved

without violating the pinch constraint. The slight difference between the two architectures is due to their different heat source utilization. Both cases correspond to an evaporation pressure of about 1.5 bar. A bell-shaped trend is observed, where an optimal intermediate pressure balances the compression work, beyond which increased irreversibility leads to a decrease in COP. Overall, these conditions lead to a temperature lift of ~100 K and a pressure ratio of ~12.8.

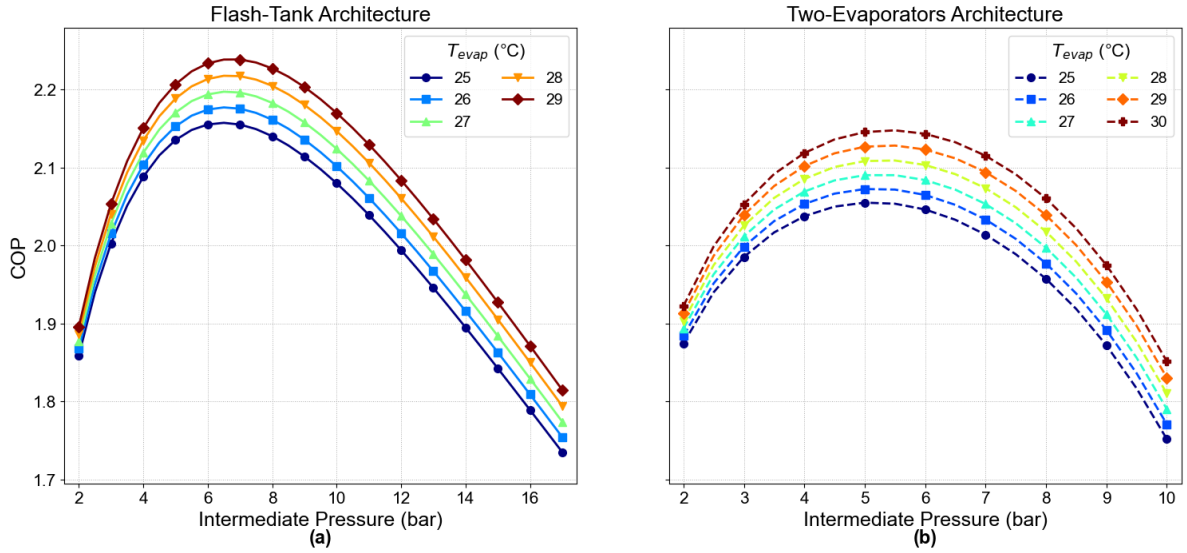

Figure 6. Optimal Evaporation Temperature (a) Flash-Tank Architecture; (b) Two-Evaporators Architecture

2.4.5 Evaluation Criteria

System performance is evaluated in terms of COP and total exergy loss, and the optimal condition is identified by simultaneously maximizing COP and minimizing total exergy loss. The intermediate pressure is optimized. In the flash-tank configuration, it corresponds to the flash tank pressure, while in two-evaporators architecture, it is defined by the saturation pressure of the intermediate evaporator. The intermediate pressure therefore determines the operating temperature level of the injected vapor and influences the thermodynamic performance of the cycle. Accordingly, it varies parametrically in the analysis. For the two-evaporators architecture, the intermediate pressure is limited to approximately 10 bar due to the finite availability of recoverable heat from the OHC hot stream. Beyond this point, the saturation temperature of the intermediate evaporator is higher than the OHC hot stream's inlet temperature as illustrated in Fig.5. Thus, no additional heat can be supplied to the second evaporator, and the system effectively behaves as a single-evaporator configuration. The energy performance of the system is evaluated using COP at different intermediate pressure levels using Eq. (1).

Exergy analysis is performed in SI units based on the control volume shown in Fig. 7, including the heat pump unit and associated heat recovery interfaces, with reference conditions of 25 °C (298.15 K) and 1.013 bar.

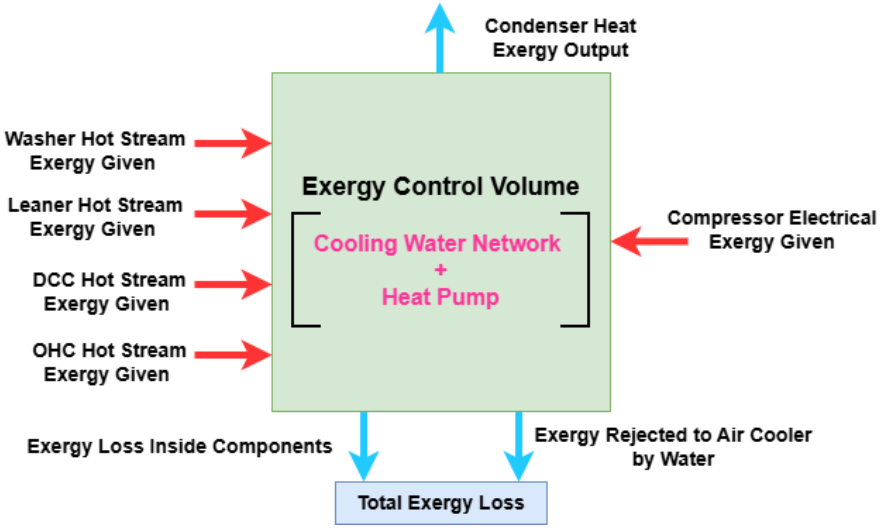

Figure 7. Control Volume of Exergy Analysis

The exergy input consists of the thermal exergy supplied by the process hot streams and the electrical exergy input to the compressor, while the useful exergy output is delivered at the condenser to meet the reboiler heat demand. Input exergy by compressor is equal to the electrical power input. The combined cooling water going to the heat exchangers inside the control volume is considered as inlet exergy and the combined cooling water coming out of the control volume after passing evaporator is considered as outlet exergy. In between it passes through the air cooler and rejects exergy as equal to the difference between the inlet and outlet exergy of the combined cooling water, and thus exergy rejected at the air cooler is considered as loss as it has not been harnessed. The exergy associated with the combined cooling water rejected to the air cooler and the exergy destruction at each component are together considered as lost exergy. In the four process heat exchangers, the hot streams provide the same amount of heat regardless of architecture as illustrated in Fig. 2. Therefore, the difference between the inlet and outlet stream exergy of the hot stream is considered as exergy given. Exergy balances are performed at the component level, including the process stream heat exchangers, heat pump components, cooling water mixing, refrigerator vapor mixing in the compressor at intermediate pressure, and exergy rejected at air cooler. The exergy difference between all inlets and outlets of a component are considered the exergy loss in that component. For any given stream the equation is as below.

$$Exergy\ In - Exergy\ Out = (Enthalpy\ In - Enthalpy\ Out) - 298.15 * (Entropy\ In - Entropy\ Out) \quad (2)$$

Consequently, the total exergy loss is obtained by summing the contributions of all components exergy loss and exergy rejected by combined cooling water to the air cooler as shown in Fig. 7. Thus, with the exergy balances shown in Fig. (7) the following simplified equation can be found.

$$\sum Exergy\ Loss = \sum Hot\ Stream\ Exergy\ Given + Compressor\ Exergy\ Input - Condensr\ Exergy\ Output \quad (3)$$

As mass flow rate is used, therefore, the exergy values are expressed in kW like the analysis of the energy section.

3. Results

3.1. Energy

For the energy analysis, along with Eq. (1), the following equation has been followed.

$$Condenser\ Heating\ Capacity = Total\ Evaporator\ Heat + Total\ Compressor\ Power\ Input \quad (4)$$

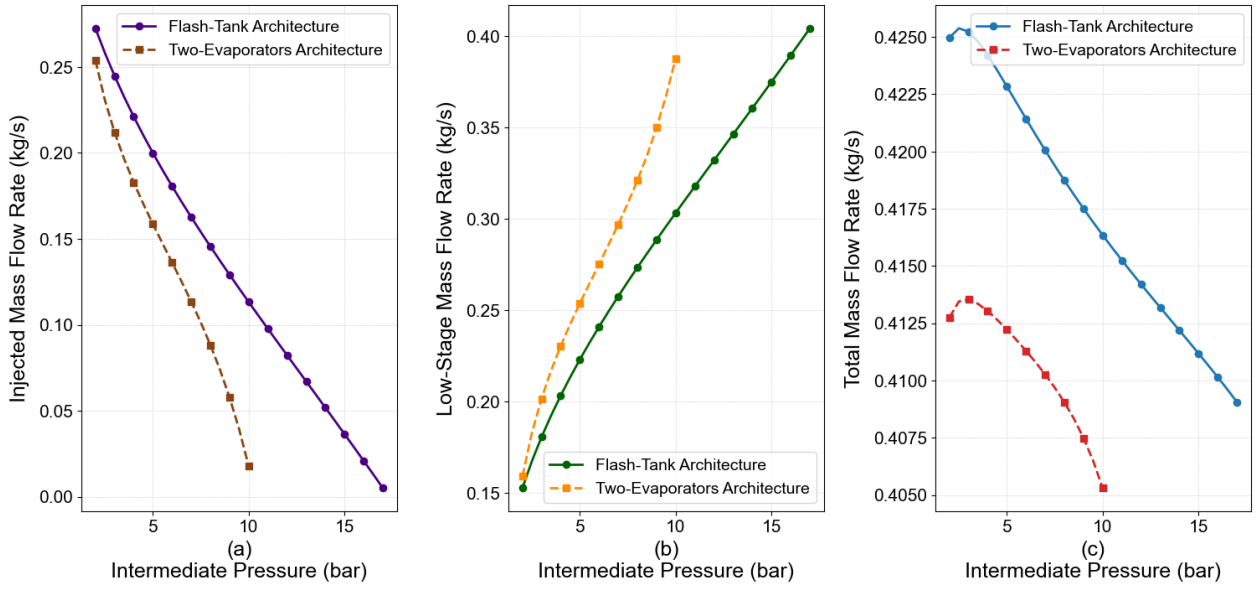

Figure 8. Refrigerant Mass Flow Rate: (a) Injected Mass Flow; (b) Low-Stage Mass Flow; (c) Total Mass Flow

The total mass flow rate and its branching was demonstrated in Fig. 3. Figure 8(a) shows that the injected mass flow rate at intermediate pressure decreases with increasing intermediate pressure for both configurations. In the flash-tank architecture, this trend results from the reduced amount of vapor generated at higher intermediate pressures. In other architecture, the decrease is governed by the progressive reduction in recoverable heat from the intermediate OHC stream as illustrated in Fig. 5, which limits the amount of vapor that can be generated in the intermediate evaporator. Beyond approximately 10 bar, no intermediate heat is available as mentioned in Section 2.4.5, and the intermediate mass flow rate becomes zero, and thus all the refrigerant is flowing through the low-temperature evaporator.

Nevertheless, Fig. 8(b) shows the low-stage mass flow rate variation with intermediate pressure. This is the mass flow that goes to the low-temperature evaporator in the two-evaporators configuration or in the single evaporator in flash-tank architecture as illustrated in Fig. 3. Figure 8(a) shows that low-stage mass flow rate rises when the intermediate pressure rises in both systems. The reason is explained by Fig. 8(c). Figure 8(c) shows that the total mass flow rate of the refrigerant is almost similar (0.4-0.42 kg/s) as the total pressure ratio and condenser duty is similar. Therefore, any decrease in the injected mass flow rate should be balanced out by an increase in the low-stage mass flow rate. Such a balancing act is needed to ensure that the condenser's duty remains the same, resulting in a steady heating capacity.

The compressor power variation is depicted in Fig. 9. The low-stage to intermediate-stage compressor power means the power needed to compress low-stage mass flow from evaporator/low-temperature evaporator pressure to intermediate pressure, while intermediate-stage to high-stage compressor power means the power needed to compress total mass flow after mixing from intermediate pressure to condenser pressure. Figure 9(a) shows that the low-stage to intermediate-stage compressor power increases with intermediate pressure in both configurations. This is because of the increase in compression ratio and also due to the increase in low-stage mass flow rate as illustrated in Fig. 8(b). In contrast, Fig. 9(b) shows that intermediate-stage to high-stage compressor power decreases with increasing intermediate pressure as the pressure ratio is decreased. As a result, the total compressor power exhibits a reversed bell-shaped curved with a clear minimum value as illustrated in Fig. 9(c). The total compressor power first decreases and then increases with intermediate pressure due to the trade-off between increasing low-stage to intermediate-stage compression work and decreasing intermediate-stage to high-stage compression work.

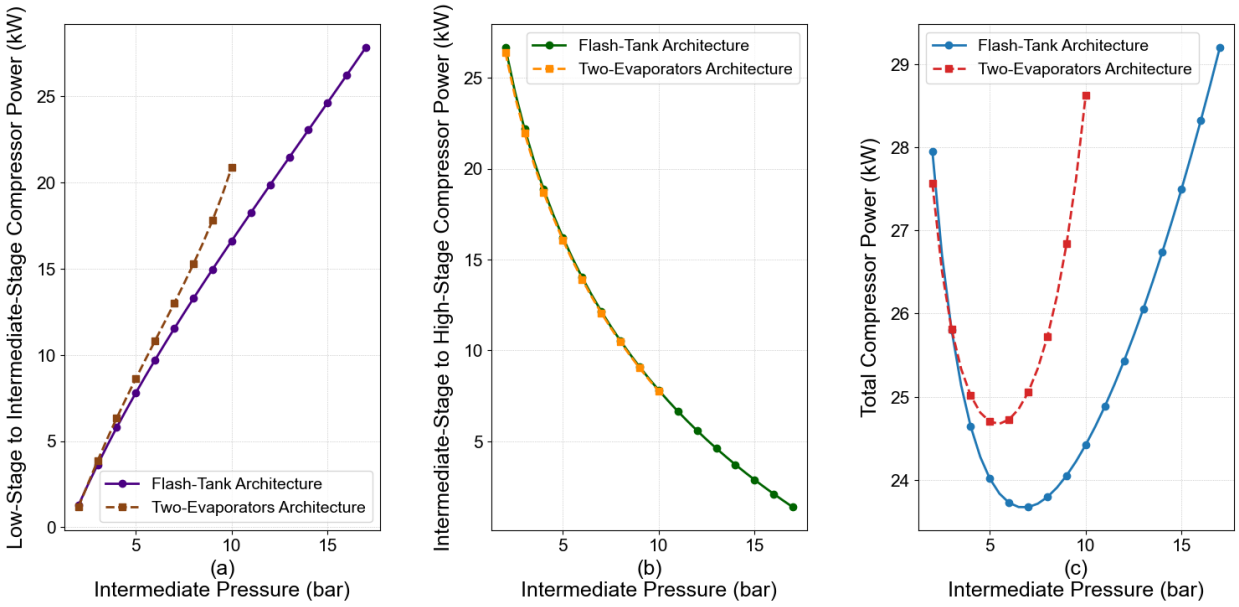

Figure 9. Compressor Power Input vs Intermediate Pressure

Total evaporator heat duty across intermediate pressure is shown in Fig. 10.

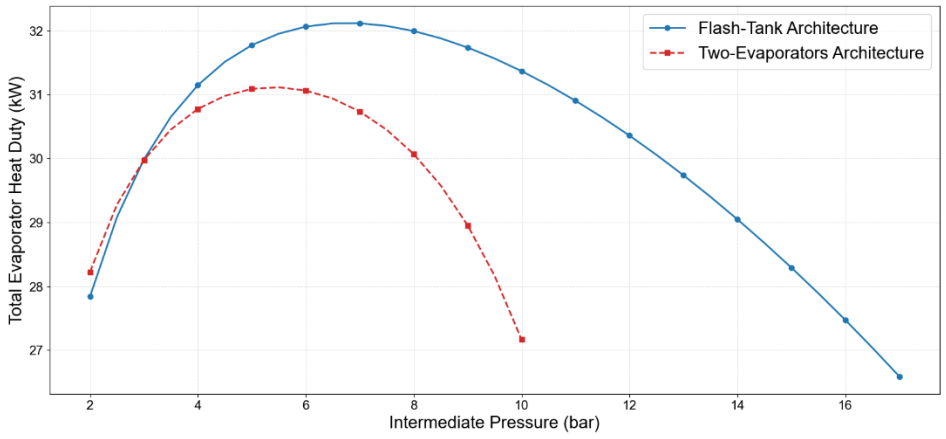

Figure 10. Total Evaporators Heat Duty vs Intermediate Pressure

For a fixed condenser heat duty, the evaporator heat duty varies inversely with compressor work according to Eq. (4). Therefore, a bell-shaped curve is observed. This trend is inverse to the compressor power curve as illustrated in Fig. 9.

The COP variation is demonstrated in Fig. 11. Since the condenser heating capacity is fixed, therefore the COP is inversely proportional to total compressor electrical power input. Therefore, the COP curve emulates bell-shaped curve or reverse of the total compressor power curve as illustrated in Fig. 9(c). Overall, during almost all operating ranges, flash-tank architecture exhibits higher COP (optimal around 7 bar) than two-evaporators architecture (optimal around 5.5 bar). One thing to mention, the power consumption to air cooler has not been included in this analysis, as this is the COP for heat pump only. However, a higher COP results in lower compressor work and increased heat recovery at the evaporator as shown in Fig. 9 and Fig. 10. Thus, the cooling water carries less residual heat to the air cooler, leading to a reduced cooling load and lower electricity consumption in the air cooler section. Therefore, even if it were included, the air cooler electricity consumption would not change the COP nature of the system.

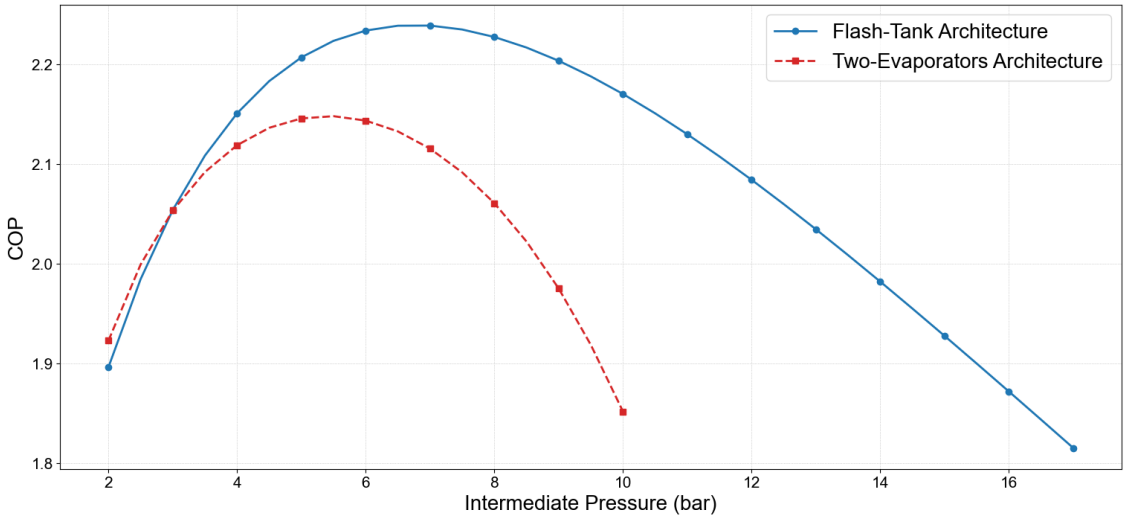

Figure 11. COP vs Intermediate Pressure

3.2 Exergy

The total exergy loss is illustrated in Fig. 12 as below.

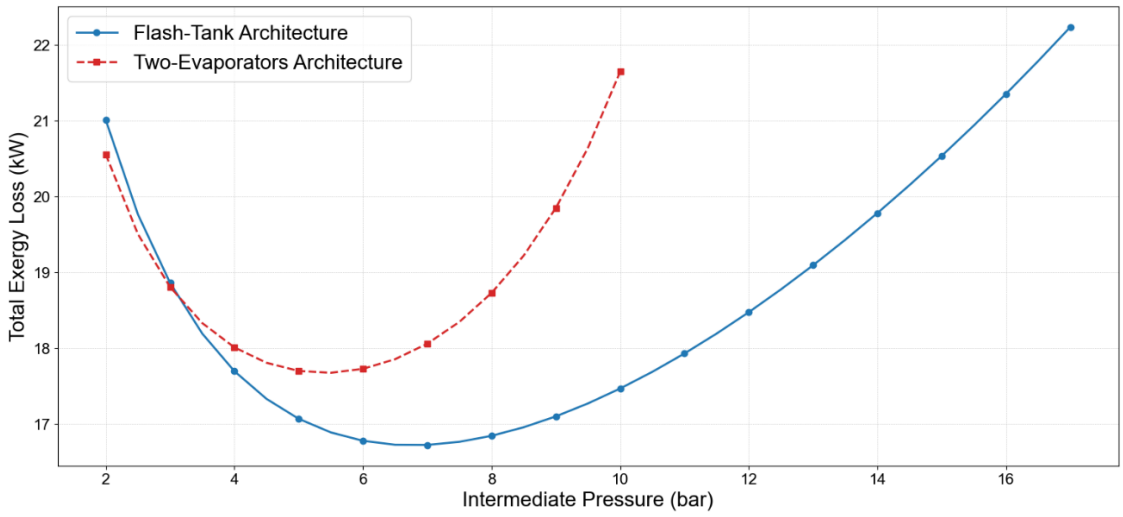

Figure 12. Total Exergy Loss vs Intermediate Pressure

As mentioned in Section 2.4.5, the exergy delivered at the condenser is imposed to remain nearly similar (~13.8 kW) across all operating conditions, with only minor variations due to changes in compressor discharge

temperature and slight variations in total refrigerant mass flow rate. Similarly, the total exergy supplied or given by the hot process streams (~6.7 kW) is essentially fixed for all cases as mentioned in Section 2.4.5. Therefore, according to Eq. (3), the compressor contribution becomes dominant, as compressor electrical power input equals compressor exergy input. According to Eq. (3), complying with exergy balance, total exergy loss is proportional to compressor exergy or power input. As the two-evaporators architecture has a higher total compressor power input than the flash-tank architecture for varied intermediate pressure as illustrated in Fig. 9(c), therefore, two- evaporators architecture has higher total exergy loss than flash-tank architecture at almost all operating intermediate pressure. Consequently, the variation of total exergy loss curve follows a trend similar to that of the compressor power and is inversely related to the COP, with minimum exergy loss corresponding to maximum system performance. Similar to the COP analysis, the flash-tank architecture exhibits a minimum exergy loss at an optimal intermediate pressure of around 7 bar, whereas the two-evaporators architecture reaches its optimum at approximately 5.5 bar (Fig. 11). Both COP and exergy-based evaluations identify the same optimal operating points and consistently indicate that the flash-tank architecture performs better over most intermediate pressure conditions. Notably, even at 5.5 bar, the flash-tank configuration achieves a higher COP and lower total exergy loss than the two-evaporators architecture at its own optimum as shown in Fig. 11 and Fig. 12 respectively.

The exergy loss analysis has been conducted using Eq. (2) for the Fig. 11. However, more microscopic component level exergy loss analysis could be compared. The component-wise exergy losses for the selected operating conditions are presented in Fig. 12. For this analysis, the optimum at 5.5 bar for the two-evaporators architecture and the optimum at 7 bar for the flash-tank architecture have been selected. The total exergy loss is lowest for the flash-tank architecture at 7 bar, while the two-evaporators architecture at 5.5 bar shows the highest irreversibility. The water-mixing, and other auxiliary losses remain comparatively smaller than the evaporators, compressor and expansion valve contributions.

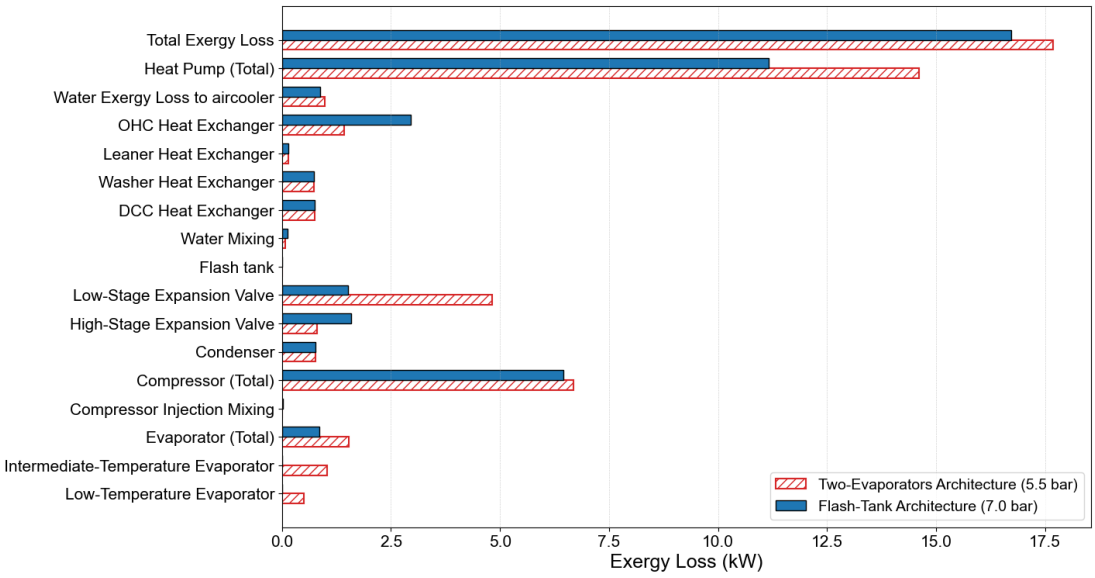

Figure 13. Component-Wise Exergy Loss at Optimal Intermediate Pressure for Both Architectures

Regarding DCC, Leaner, Washer, these three heat exchangers have similar streams with similar thermal condition for all simulations and thus the exergy loss is the same in all cases. However, a clear difference between the two architectures appears on the OHC side. The OHC-related exergy loss is lower in two-evaporators architecture because part of the OHC heat is recovered directly in the intermediate-temperature evaporator at a higher temperature level before the remaining heat is transferred to the cooling-water loop. This improves the quality of heat recovery and reduces the irreversibility associated with cooling the OHC hot stream only through the coolant water loop like in the other architecture. One thing to mention is that in Fig. 12, for flash-tank architecture, the OHC exergy loss means loss in cooling-water OHC heat exchanger. For two-evaporators architecture, it includes both the losses in the intermediate-temperature evaporator and the OHC cooling-water heat exchanger, so that the comparison reflects the benefit of recovering OHC heat at two temperature levels.

However, total evaporator loss is higher for two-evaporators architecture. In this architecture, though the heat is recovered at high-temperature level at intermediate-temperature evaporator, the exergy loss is high as well. The reason is the inlet and outlet thermodynamic conditions of hot streams and injected mass flow. At 5.5 bar the saturation temperature of the intermediate-temperature evaporator is around 72.8°C. The inlet of the injected mass flow rate at this evaporator is in two phases after going through expansion valve and it leaves as superheated vapor as shown in Fig. 3. However, because of 5K pinch, the outlet temperature of the OHC

hot stream is 77.8°C. Therefore, the hot stream provides significant amount of heat over a temperature range from 105°C to 77.8°C as shown in Fig. 5. Despite the fact that both fluid flows are in a higher temperature state, the process takes place at a definite temperature gradient across the heat exchanger. More importantly, the hotter stream is releasing heat energy at a better quality than the refrigerant is capable of capturing. Heat absorption takes place via evaporation and partial superheat, which leads to an increased level of irreversibility or entropy of the process. Therefore, the exergy increase of the refrigerant is less compared to the exergy decrease by the hot OHC stream, and thus the higher loss.

For flash-tank architecture, there is only one evaporator, and its contribution has been reflected in Evaporator (Total) section in Fig 12. For the two-evaporators architecture, the low-temperature evaporator saturation temperature varies slightly, however the mass flow rate varies compared to the other architecture. Between these, the low-temperature evaporator exergy loss for two-evaporators architecture is less compared to single evaporator of the flash-tank architecture, as less heat is transferred at this low temperature. However, the total evaporator exergy loss including both evaporators is higher for two-evaporators architecture compared to flash-tank architecture.

For both architectures, the low-temperature evaporator's operating saturation temperature varies slightly, and the amount of extracted exergy varies as well but not significantly. However, because of having two evaporators, two-evaporators architecture cannot extract more heat at low-temperature evaporator compared to the single evaporator in flash-tank architecture. Therefore, the exergy rejected by water to air cooler is slightly higher in two-evaporators architecture.

The expansion valve losses must also be interpreted according to the actual expansion paths. The high-stage expansion valve loss does not vary significantly because, in two-evaporators configuration, only the injected mass flow expands from the condenser outlet to the intermediate pressure, whereas in other architecture the total mass flow passes through this valve as shown in Fig. 3. Therefore, flash-tank architecture has higher loss in this component. In contrast, the low-stage expansion valve loss is much higher in two-evaporators architecture. Because in flash-tank architecture, the low-stage expansion occurs only for the low-stage mass flow from intermediate pressure to evaporating pressure as shown in Fig. 3. However, for two-evaporators architecture, the low-stage mass flow going to the low-temperature evaporator expands directly from condensing pressure to evaporating pressure, and thus the much larger pressure drops leads to significantly higher exergy loss.

For flash-tank architecture, the total compressor exergy loss is lower than two-evaporators architecture as discussed earlier in Fig. 12.

Overall, for both architectures, total individual components level exergy loss and exergy rejected by water to air cooler is equal to the total exergy loss as explained in Fig. 11 using Eq. (3). This agreement confirms that the two approaches, such as summing component-wise exergy and the overall system boundary exergy balance using Eq. (3) are fully consistent.

4. Conclusion

The results depict that the system performance is strongly influenced by the intermediate pressure, with an optimal range around 5–7 bar. Flash-tank architecture consistently achieves higher COP and lower total exergy destruction compared to two-evaporators architecture in almost all operating intermediate pressure points. Although two evaporators enable improved heat recovery from the OHC stream at higher temperature levels, this advantage is offset by increased exergy destruction in the other components of the heat pumps, especially in the expansion processes, particularly due to the larger pressure drop across the low-stage expansion valve. Overall, the total exergy loss closely follows the trend of compressor power, confirming the inverse relationship with COP. Consequently, the optimal intermediate pressure corresponds to compressor work for which at the same point both maximized COP and minimized total exergy loss are observed for both architectures. These findings demonstrate that, for the given process conditions, the flash-tank configuration provides a more efficient and practical solution for heat integration in this particular CO_2 capture system.

Accordingly, from this investigation, it cannot be concluded that using higher temperature levels for capturing waste heat will necessarily enhance system efficiency. It also depends on the available total heat as a portion of the total heating capacity at intermediate temperature, and temperature profile of both fluids operating at this evaporator. While, indeed, the two-evaporators architecture allows for higher temperature levels for capturing heat, the same setup also introduces irreversibility caused by temperature differences and the state of the refrigerant, hence causing more exergy destruction. Overall, this investigation demonstrates that apart from the temperature level of waste heat available for use, high-temperature heat pump efficiency for capturing CO_2 in solvents also relies heavily on its ability to match the heat source and heat sink efficiently. This consideration is especially relevant when dealing with waste heat sources with varying temperature distributions, and also with higher reboiler temperatures.

To validate the model results, a test bench is being under construction at the University of Liege. Moreover, the evaporation temperature was selected based on 5K superheat; nevertheless, in reality we might need higher superheating so that we can ensure dry suction at the inlet of the compressor. In that regard, in real

operation the saturation temperature might be lower than 29°C. In addition, the maximum discharge temperature of the compressor is mentioned to be 135°C by the manufacturer; however, for the optimal intermediate pressure the discharge temperature is around 140°C via simulation. It is expected that the compressor might be able to withstand these few degrees above its mentioned temperature in real life; otherwise, the condensation temperature might be adjusted a few degrees lower, and the simulation model has to be adapted to account for the constraints. However, the COP and total exergy loss is expected to not change significantly, though because of new total pressure ratio the optimal intermediate pressure might vary.

Acknowledgments

The project is funded by Win4Excellence EFES, Wallonia, Belgium

References

[1] United Nations. Paris Agreement – Available at: <https://www.un.org/en/climatechange/paris-agreement> [accessed 26.03.2026].

[2] Council of the European Union. Climate change: what the EU is doing – Available at: <https://www.consilium.europa.eu/en/policies/climatechange/> [accessed 26.03.2026].

[3] Beguin B. Simulation and adaptation of a biomass combined heat and power plant [MSc thesis]. Liège, Belgium: Université de Liège; 2022.

[4] Bui M., Adjiman C.S., Bardow A., Anthony E.J., Boston A., Brown S., Mac Dowell N. Carbon capture and storage (CCS): the way forward. Energy Environ Sci 2018;11(5):1062–1176.

[5] International Energy Agency. Carbon capture, utilisation and storage – Available at: <https://www.iea.org/energy-system/carbon-capture-utilisation-and-storage> [accessed 26.03.2026].

[6] Johansson J.S. Heat supply alternatives for CO_2 capture in the process industry. Int J Greenhouse Gas Control 2012;8:217–232.

[7] Baudoux A., Demeyer F., De Paepe W. Advanced configurations of amine-based post-combustion carbon capture process applied to combined cycle gas turbine. Energy Convers Manag X 2024;22:100537.

[8] Beguin B., Van Lierop T., Léonard G. Optimal integration of a high-temperature heat pump in a CO_2 capture pilot plant. In: Carnot 2024 – Belgian Symposium of Thermodynamics; 2024; Belgium.

[9] Arpagaus C., Bless F., Uhlmann M., Schiffmann J., Bertsch S.S. High-temperature heat pumps: market overview, state of the art, research status, refrigerants, and application potentials. Energy 2018;152:985–1010.

[10] Mateu-Royo C., Navarro-Esbrí J., Mota-Babiloni A., Amat-Albuixech M., Molés F. Theoretical evaluation of different high-temperature heat pump configurations for low-grade waste heat recovery. Int J Refrig 2018;90:229–237.

[11] Arpagaus C., Prinzing M., Kuster R., Bless F., Uhlmann M., Schiffmann J., Bertsch S.S. High-temperature heat pumps – theoretical study on low GWP HFO and HCFO refrigerants. In: Proceedings of the 25th IIR International Congress of Refrigeration; 2019 Aug 24-30; Montreal, Canada.

[12] Tello-Oquendo F.M., Navarro-Peris E., Gonzálvez-Maciá J. Comparison of the performance of a vapor-injection scroll compressor and a two-stage scroll compressor working with high pressure ratios. Appl Therm Eng 2019;160:114023.

[13] Sartor K. Développement d'un outil de simulation et d'analyse technico-économique et environnementale d'un réseau de chaleur [PhD thesis]. Liège, Belgium: Université de Liège; 2018.

[14] Molina-Fernández C., Kreit P., Beguin B., Bekhti S., Calberg C., Kalbusch J., Léonard G. An automated CO_2 capture pilot plant at ULiège: a platform for the validation of process models and advanced control. Syst Control Trans 2025;4:423–429.

[15] Jensen E.H., Andreasen A., Jørsboe J.K., Andersen M.P., Hostrup M., Elmegaard B., Riber C., Fosbøl P.L. Electrification of amine-based CO_2 capture utilizing heat pumps. Carbon Capture Sci Technol 2024;10:100154.

[16] Janod T., Chaudoir B., Cendoya A., Lemort V. Organic Rankine cycle with or without thermal energy storage: a ceramic plant case study. In: ECOS 2025: Proceedings of the 38th International Conference on Efficiency, Cost, Optimization, Simulation and Environmental Impact of Energy Systems; 2025 Jun 29-Jul 4; Nice, France.

[17] Wu D., Wei J., Hu B. Theoretical analysis, experimental research and industrial verification of a high-temperature heat pump based on R1233zd(E). Energy 2025;319:135175.

[18] Koundinya S., Jothilingam J., Martin S.R., Seshadri S. Numerical and experimental study of a 120 °C heat pump using a scroll compressor. In: International Conference on Compressors and their Systems; 2023 Sep 11; p. 327–338. Cham, Switzerland: Springer Nature.